Applied Thermal Engineering 88 (2015) 71–81

Contents lists available at ScienceDirect

Applied Thermal Engineering

journal homepage: www.elsevier.com/locate/apthermeng

Numerical study on drag reduction and heat transfer enhancement in microchannels with superhydrophobic surfaces for electronic cooling

Yongpan Cheng [a], Jinliang Xu [a,*], Yi Sui [b]

[a] School of Energy Power and Mechanical Engineering, North China Electric Power University, Beijing 102206, China
[b] School of Engineering and Materials Sciences, Queen Mary University of London, Mile End Road, London E1 4NS, UK

GRAPHICAL ABSTRACT

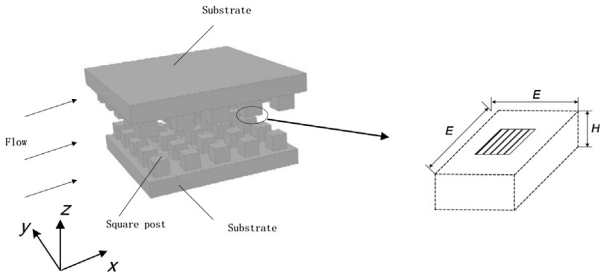

ARTICLE INFO

Article history:
Received 9 June 2014
Received in revised form
19 August 2014
Accepted 17 October 2014
Available online 25 October 2014

Keywords:
Superhydrophobic surfaces
Electronic cooling
Goodness factor
Numerical Study

ABSTRACT

Microchannels with superhydrophobic surfaces are a promising candidate for electric cooling with mild frictional penalty. Frictional and thermal performance of laminar liquid-water flow in such microchannels is numerically investigated for various shear-free fractions and Reynolds numbers. The structures on superhydrophobic surfaces include square posts and holes, transverse and longitudinal grooves. Combined frictional and thermal performance of microchannels is evaluated by a goodness factor, and is compared with that of smooth plain channels. It is found that with increasing shear-free fractions, both friction factor and average Nusselt number deteriorate for four surface patterns; however, goodness factor is improved significantly over smooth plain channels. In general, superhydrophobic surfaces containing longitudinal and transverse grooves exhibit the lowest and highest frictional and thermal performance, respectively; however, combined performance of these two are on opposite. Among four surface patterns, longitudinal grooves have the highest goodness factors, except at high shear-free fractions or high Reynolds numbers where overall performance is surpassed by square posts. At very low or high shear-free fractions, frictional and thermal performance of two-dimensional square posts and holes approaches that of one-dimensional longitudinal or transverse grooves. Our study suggests microchannels with superhydrophobic surfaces as promising candidates for efficient cooling devices.

1. Introduction

Temperature plays a crucial role in the operation of electrical devices. For example, a rise of 2 °C in temperature will reduce the reliability of a silicon chip by about 10% [1]. It is thus very important to find effective solutions of heat removal for electrical devices. With the increase of power density and the miniaturization of electronic packages, conventional cooling approaches employing air as coolant is not able to meet the cooling demand. Since the classical experimental work by Tuckerman and Pease [2], who described superior cooling capability for extremely high power density devices, direct liquid cooling incorporating microchannels

* Corresponding author. Tel.: +86 10 61772268.
E-mail address: xjl@ncepu.edu.cn (J. Xu).

http://dx.doi.org/10.1016/j.applthermaleng.2014.10.058
1359-4311/

has been gaining extensive attention, as reviewed by Garimella and Sobhan [3] and Hassan et al. [4]. Conventional microchannel heat sinks usually employ straight channels, in which the heat transfer is not very efficient. Various approaches have been proposed to improve the heat transfer performance of microchannel heat sinks by introducing complicated channel geometries, for example by using wavy channels [5–7], zigzag channels [8], or fractal-like branching channels networks [9], tree-shape microchannels nets [10], coiled or even hybrid-geometry channels [11]. However, the trade-off is that the required pressure gradient to drive the liquid coolant through microchannels also increases significantly and can become prohibitive with the decrease of the channel dimension. Therefore, it is of vital importance to seek an effective methodology to reduce the required pressure gradients to reasonable levels. Superhydrophobic surfaces are promising candidates for meeting this requirement; however, its potential for incorporation into microchannel heat sinks has not been well explored so far.

Superhydrophobic surfaces are usually formed by patterning micro- or nano-posts, holes or grooves on a solid substrate surface, as shown in Fig. 1, followed by treating the surface-textured substrates with a thin hydrophobic layer. If the cavity size between the patterned elements is sufficiently small, such as at the order of microns or even smaller, the liquid flowing through the channel will not penetrate the cavities, and a Cassie or dewetted state is thus maintained. A pocket of air or vapor is trapped in the cavity, and thus the effective contact area between the flowing liquid and the solid wall is reduced, as well as required pressure gradient across the microchannel.

There have been numerous previous research efforts mainly targeted at investigating the hydraulic performance of superhydrophobic surfaces patterned with different geometries. Philip [12,13] employed the conformal mapping technique to analyze the laminar flow through a circular tube with longitudinal grooves modeled as shear-free stripes, and significant reduction in flow resistance was observed. Similar reduction was verified by the experimental work in microchannels patterned with longitudinal grooves by Ou and Rothstein [14] as well as Maynes et al. [15].The superhydrophobic surfaces exhibit different effective slip performance if the grooves are oriented transversely, and these were investigated analytically [16–19], numerically [15,20] and experimentally [21,22]. All previous investigations have shown consistently that the flow resistance for channels with longitudinal grooves is always lower than that for transverse grooves, regardless of the driving mechanism which is either pressure-driven or shear driven flows.

Besides grooves, superhydrophobic surfaces containing post or hole patterns can also serve as effective means for reducing the flow resistance in microchannels [23–25]. Amongst these studies Ybert et al. [25] systematically derived scaling laws to investigate the flow resistance corresponding to different shear-free fractions for patterned geometries including square posts, square holes and grooves. However, their study is limited to Stokes flow regime. Till now, there is no systematic study of the frictional performance of microchannels with various superhydrophobic patterns by taking into account the effect of inertia, although inertial effect on individual patterns has been considered [20,26,27].

Furthermore, up to date, the study of thermal performance in microchannels containing superhydrophobic surfaces has been rather limited. To our best knowledge, the only study was carried out by Maynes et al. [28] using numerical simulation. They explored the laminar flow and thermal transport in a microchannel patterned with periodically repeating transverse ribs at constant wall temperature, and found that the thermal performance deteriorates with increasing relative groove length, increasing relative rib/groove module length or decreasing Reynolds numbers, and furthermore, the thermal-hydraulic performance of the patterned microchannel investigated is superior to the classic parallel plate micro-channel over a large range of parameters investigated. So far, there is no systematic study of the thermal performance of microchannel heat sinks with various superhydrophobic patterns, and the combined hydraulic and thermal performance is also largely unknown. The objective of this work is thus to systematically investigate the frictional and thermal performance of laminar liquid-water flow in microchannels with superhydrophobic surfaces with various geometries including longitudinal and transverse grooves, square posts and square holes at different flow Reynolds numbers and shear-free fractions.

In the following sections, the physical model and numerical formulation will first be explained. This will be followed by a discussion concerning the influence of shear-free fraction and Reynolds number on the frictional and thermal performance in microchannels patterned with four different geometries of superhydrophobic surfaces. After that, the combined frictional and thermal performance is evaluated in terms of the goodness factor under different shear free fractions and flow Reynolds numbers. Finally some conclusions will be drawn based on comparison of frictional, thermal and combined performance for four different surface patterns and smooth plain microchannel. These results may be useful for the design of microchannel-based heat sinks containing superhydrophobic surfaces.

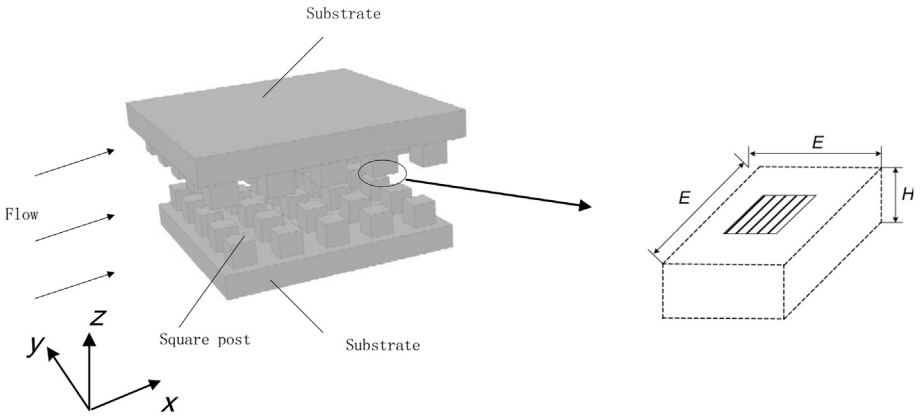

Fig. 1. Schematic of straight channel patterned with square posts.

2. Mathematical formulation

In Fig. 1 a schematic diagram of a straight microchannel containing superhydrophobic surfaces is shown. Take the square posts as example, the square posts are patterned in-line on both the upper and lower walls of the microchannel with height of $2H$, and they are arranged on a square lattice with the edge length of E. A square post region in the upper wall of microchannel is enlarged in the right diagram of Fig. 1, and it is shown that the hatched region represents the solid post or no-slip region, whereas the unshaded region corresponds to the gas region. The capillary number $Ca = \mu U_{\text{in}}/\sigma$ of the flow in the microchannels is assumed to be sufficiently small, where σ is the surface tension of water. This implies that viscous forces are negligible compared to surface tension forces, and that the deformation of the water–air interface is negligible. Hence, the air–water interface can be assumed to be flat. Due to low thermal conductivity and viscosity of air compared with water, water–air interface can be regarded as shear-free and adiabatic. For simplification the water flow region in the microchannels is taken as the computational domain, excluding air region in the cavity. The x-direction is liquid flow direction where a pressure gradient is applied to drive the flow, the y-direction is transverse to the flow direction, and the z-direction is parallel to the direction of the channel height, the origin is located at the center of mid-plane normal to z direction. The square posts are arranged in a periodic array along both the x- and y-direction, therefore flow in the microchannels becomes periodically developed in the x-direction and is symmetric in the y-direction. Besides square posts, several other geometric configurations, such as, transverse grooves and longitudinal grooves, square holes have also been studied for performance comparison in this work, as shown in Fig. 2. Due to the symmetry and periodicity of the geometric configurations, the computational domain can be simplified [20,28], which is chosen as the region bounded by dashed lines in the x–y plane from the mid-plane of the channel to the upper wall in the z-direction, as shown in Fig. 1. The flowing liquid in the microchannel is considered as liquid water with the inlet temperature of 293 K and an absolute pressure of 1 atm, the governing equations are given as follows:

Continuity equation:

$$\frac{\partial}{\partial x_i}(\rho u_i) = 0 \tag{1}$$

Momentum equation:

$$\frac{\partial}{\partial x_i}(\rho u_i u_k) = \frac{\partial}{\partial x_i}\left(\mu \frac{\partial u_k}{\partial x_i}\right) - \frac{\partial p}{\partial x_k} \tag{2}$$

Energy equation

$$\frac{\partial}{\partial x_i}(\rho u_i T) = \frac{\partial}{\partial x_i}\left(\frac{\lambda}{c_p}\frac{\partial T}{\partial x_i}\right) \tag{3}$$

Other salient parameters are defined as follows:

$$\text{Relative pattern width } L = E/H \tag{4}$$

$$\text{Dimensionless shear} - \text{free fraction } \delta_g = \frac{A_g}{A_g + A_s} \tag{5}$$

$$\text{Reynolds number } Re = \frac{\rho U_{\text{in}} D_{\text{h}}}{\mu} \tag{6}$$

$$\text{Non} - \text{dimensional temperature } \theta = \frac{T - T_W}{T_b - T_W} \tag{7}$$

$$\text{Bulk temperature} \quad T_b = \frac{\int_0^H UT\mathrm{d}h}{\int_0^H U\mathrm{d}h} \tag{8}$$

$$\text{Darcy friction factor } f = \frac{\Delta P D_h}{\frac{1}{2}\rho U_{\text{in}}^2 E} \tag{9}$$

$$\text{Overall heat transfer coefficient } h = \frac{\dot{m} C_p (T_{\text{in}} - T_{\text{out}})}{E^2 \Delta T_m} \tag{10}$$

$$\text{Overall Nusselt number } Nu = \frac{hD_h}{\lambda} \tag{11}$$

$$\text{Local Fanning friction factor } f_x = \int_{-E/2}^{E/2} \frac{2\mu \frac{\partial u}{\partial z}\Big|_W}{\rho U_{\text{in}}^2} \mathrm{d}y/E \tag{12}$$

$$\text{Local Nusselt number } Nu_x = \int_{-E/2}^{E/2} \frac{\partial T}{\partial z}\Big|_w \frac{D_h}{T_b - T_w} \mathrm{d}y/E \tag{13}$$

where A_g is the area corresponding to the shear-free region (the unshaded region in Fig. 2), A_s is the area corresponding to the no-slip solid region (the hatched region in Fig. 2), Pr is the Prandtl number, D_h is the channel hydraulic diameter ($D_h = 4H$), H is half height of channel, p is the pressure, θ is the non-dimensional temperature, T_W is the wall temperature, T_{in} is the inlet bulk temperature, T_{out} is the outlet bulk temperature, ΔT_m is the log mean temperature difference. The term c_p is the specific heat capacity at constant pressure, and λ is the thermal conductivity of the fluid.

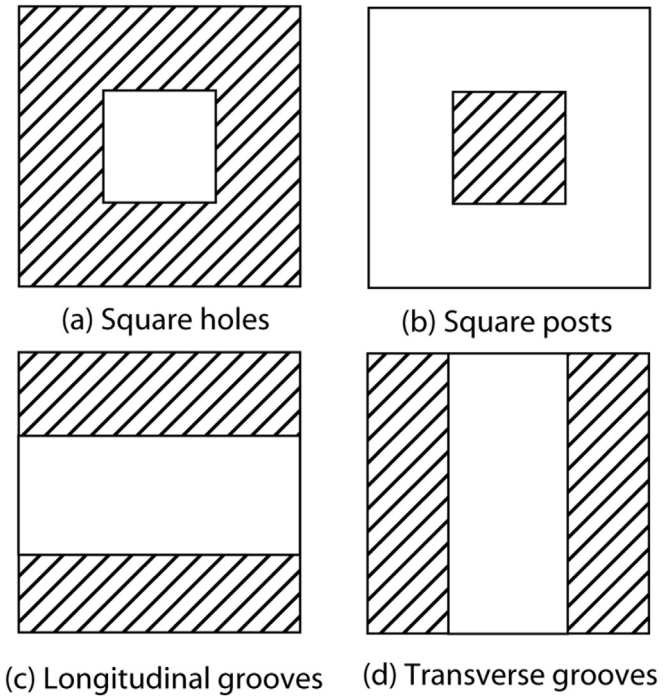

Fig. 2. Configurations of four surface patterns.

The required boundary conditions are:

At the inlet and outlet of the computational domain ($x = -E/2$ and $x = E/2$):

Periodic boundary conditions for the dimensional velocity components and non-dimensional temperature:

$$u_{in} = u_{out}, \quad v_{in} = v_{out}, \quad w_{in} = w_{out}, \quad \theta_{in} = \theta_{out} \tag{14a}$$

Along the side boundaries ($y = -E/2$ and $y = E/2$):

$$\text{Symmetrical boundary condition}: \ \frac{\partial u}{\partial y} = \frac{\partial w}{\partial y} = v = \frac{\partial T}{\partial y} = 0 \tag{14b}$$

Along the upper boundary ($z = H$):

$$\text{Solid region}: \ \text{no slip}: \ u = v = w = \theta = 0 \tag{14c}$$

$$\text{Gas region}: \ \text{shear} - \text{free}: \ \frac{\partial u}{\partial z} = \frac{\partial v}{\partial z} = w = \frac{\partial T}{\partial z} = 0 \tag{14d}$$

Along the lower boundary ($z = 0$):

$$\text{Symmetrical boundary condition}: \ \frac{\partial u}{\partial z} = \frac{\partial v}{\partial z} = w = \frac{\partial T}{\partial z} = 0 \tag{14e}$$

The governing equations are discretized using the finite volume method [29,30], central difference scheme and the stability-guaranteed second order difference (SGSD) scheme [31]are adopted to discretize the diffusion terms and convection terms, respectively. In order to improve the coupling between the pressure and the velocity so as to accelerate the convergence, the newly proposed CLEARER algorithm on collocated grid [32] is employed. As the velocity boundary condition is set for the inlet and outlet, as in Eq. (14a), the pressure boundary condition is not needed at both boundaries. For each iteration, the pressure correction equation is solved to satisfy the continuity equation for mass conservation. When the relative maximum mass residual in the computational cell is less than 1.0×10^{-9}, the iteration process for solving the flow field is terminated, and that for solving the temperature field subsequently begins. When the relative difference of total heat flux between two successive iterations is less than 1.0×10^{-8}, the solution for temperature field is considered to have converged. A non-uniform grid is adopted in order to improve solution accuracy, with finer grid spacing near regions where velocity or temperature variations are large. After a grid independence study is performed, a grid system using $122 \times 66 \times 66$ is eventually adopted in the subsequent numerical simulations for square posts and square holes. While for the transverse groove and longitudinal groove configurations, the number of grid points is reduced in the symmetrical direction due to their two-dimensional (2D) flows characteristics.

3. Results and discussion

3.1. Numerical validation

The frictional performance of micro-channels with longitudinal grooves and transverse grooves has previously been investigated analytically by Philip [12,13] and Teo and Khoo [19], respectively. Therefore, in order to validate the developed code and model, computations were carried out for the fluid flow in straight microchannels patterned with longitudinal and transverse grooves. The results are presented for a relative pattern width $L = E/H = 1.0$ in Fig. 3(a). The lines correspond to the analytical results, whereas the symbols correspond to the present numerical results. In general, reasonably good agreement is observed. For convenience, the frictional performance is expressed using the product of friction factor and Reynolds number *fRe* hereafter. When the shear-free fractions in transverse and longitudinal grooves approach zero, the channels approach a straight channel consisting of two parallel plates, and the product *fRe* approaches the asymptotic value 96 for the fully developed flow. To further validate the present model, fully developed heat transfer in the straight channel was also numerically simulated at constant wall temperature condition. When the Reynolds number is more than 100, the axial heat conduction in the fluid can be ignored, and the convective heat transfer become dominant, the Nusselt number obtained from the numerical simulation equals to7.52, which is in agreement with the theoretical value of 7.54. These results show the present model is accurate for the simulation of flow and heat transfer in microchannels.

3.2. Comparison of frictional performance

3.2.1. Effect of shear-free fractions

The flow resistance in the micro-channels is caused by the shear stress between the moving liquid and the no-slip solid wall. In Fig. 4, the frictional performance of microchannels with square posts, square holes, transverse grooves and longitudinal grooves is compared for different shear-free fractions at $Re = 1, 100$ and 1000, respectively. It is obvious that with the increasing the shear-free fractions for all four surface patterns, the frictions decrease dramatically. For the range of shear-free fractions investigated at the three different Reynolds numbers, the microchannels with longitudinal grooves almost yield the lowest frictional performance among the four surface patterns, intuitively because the flow over longitudinal grooves does not experience the periodic acceleration and deceleration at the trailing edge and leading edge of no-slip solid walls which happen for other geometries. On the contrary, in a channel with transverse grooves the flow experiences the strong acceleration and deceleration, and the overall friction is thus much larger than that in the longitudinal grooves. As the two-dimensional surface pattern of square posts and square holes can be considered as the combination of one-dimensional surface pattern of transverse grooves and longitudinal grooves, the frictional performance of microchannels with square posts and square holes lies in between that with transverse grooves and longitudinal grooves, as seen in Fig. 4.

For all Reynolds numbers, it is interesting to observe that at lower and upper limits of shear-free fractions considered, the frictional performance of microchannels with two-dimensional square posts or holes approach that of one-dimensional grooves. For example, for a shear-free fraction of $\delta_g < 0.2$, the frictional performance of microchannels with square holes and longitudinal grooves are equivalent, and for $\delta_g < 0.4$ the microchannels with square posts show almost identical frictional performance as those with transverse grooves. However, for large shear-free fractions, the frictional performance of microchannels with square holes becomes almost comparable to that with transverse grooves; similarly the frictional performance of microchannels with square posts becomes comparable to that of longitudinal grooves. The interesting phenomena can be explained as follows. For a microchannel with square posts, the shear free parts can be considered as the combination of narrow transverse gaseous grooves and longitudinal gaseous grooves at low shear-free fractions. Since longitudinal grooves produce less friction than the transverse grooves, the friction of square posts are thus mainly determined by that of transverse grooves, and so that the square posts and transverse grooves are almost equivalent under low shear-free fractions. While under high shear-free fractions, the square holes can be

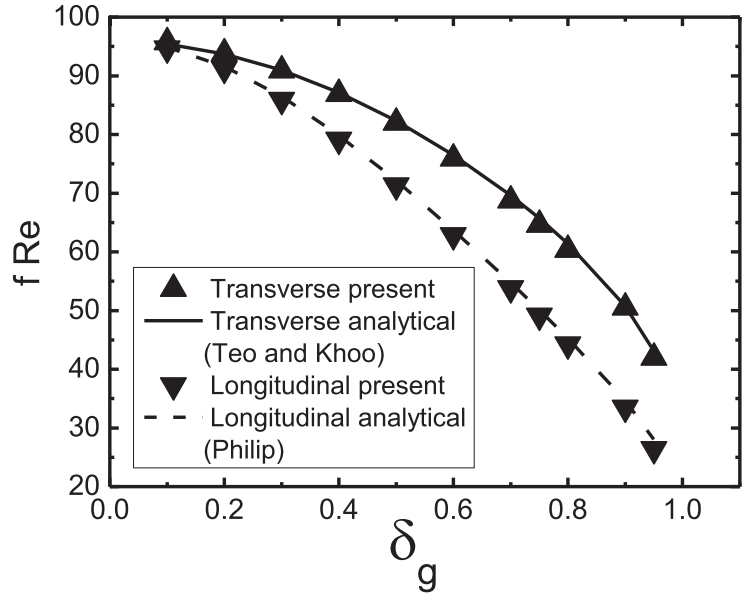

(a) Comparison of friction for transverse and longitudinal grooves at L=1.0 and Re=1.0

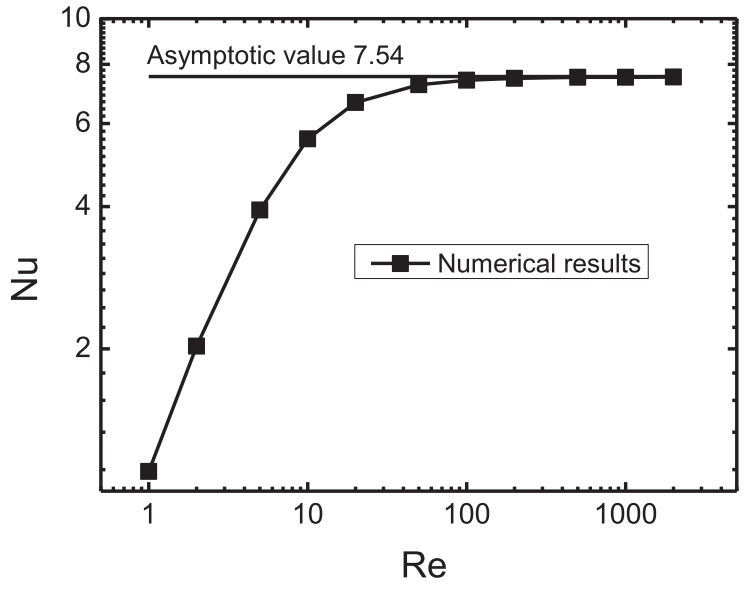

(b) Comparison of Nu numbers between two parallel plates

Fig. 3. Comparison between numerical results and analytical results.

considered as the combination of narrow transverse solid stripes and longitudinal solid stripes grooves, so the square holes and transverse grooves are almost equivalent under high shear-free fractions. For the square holes under low shear-free fractions and square posts under high shear-free fractions, they are equivalent as the longitudinal grooves, which can be explained from the viewpoint of scaling laws, as discussed by Ybert et al. [25].

Although the microchannel with longitudinal grooves always has the best frictional performance in a wide range of shear free fractions, compared with those with other three surface patterns, it is found, however, at very large shear-free fraction the microchannel with square posts exhibits a lower frictional performance if the Reynolds number is low to moderate, say less than 100. For example, at $\delta_g = 0.95$, the friction of microchannel with longitudinal grooves can be 8% higher than that of square posts, because the two-dimensional square posts have much shorter edge of solid patch along flow direction than one-dimensional longitudinal grooves under the same shear-free fractions.

3.2.2. *Effect of Reynolds numbers*

Numerical study by Davies et al. [20] shows that inertial effects have a great influence on the friction performance in microchannel patterned with transverse superhydrophobic grooves, and their effects on the global frictions are investigated as well as the effects of shear-free fraction, here the study is extended to more surface patterns, including square posts, square holes and longitudinal

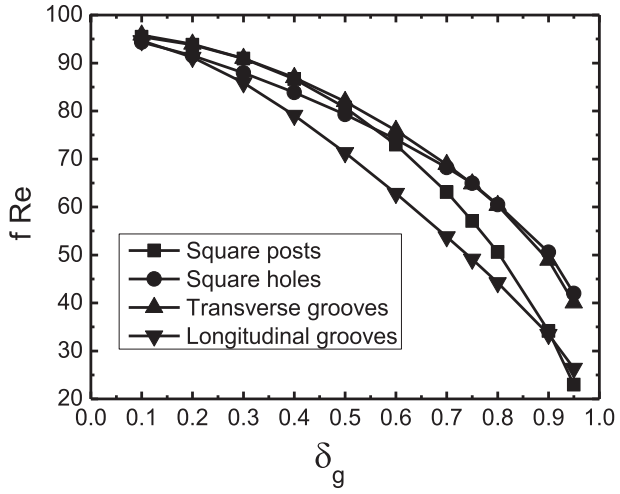

(a) Re=1

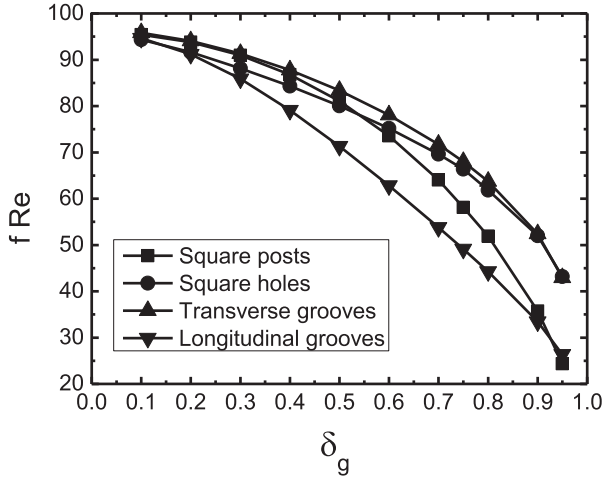

(b) Re=100

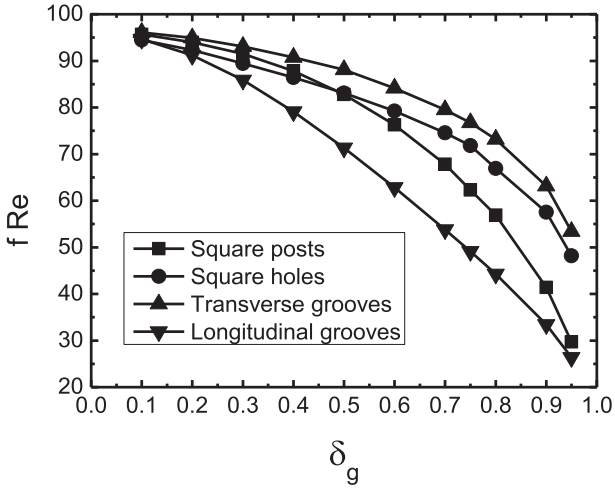

(c) Re=1000

Fig. 4. Influence of shear-free fraction on friction for four surface patterns at $L = 1.0$.

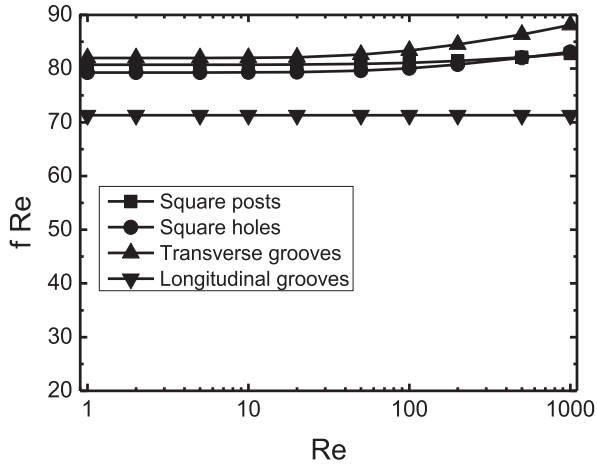

(a) $\delta_g = 0.5$

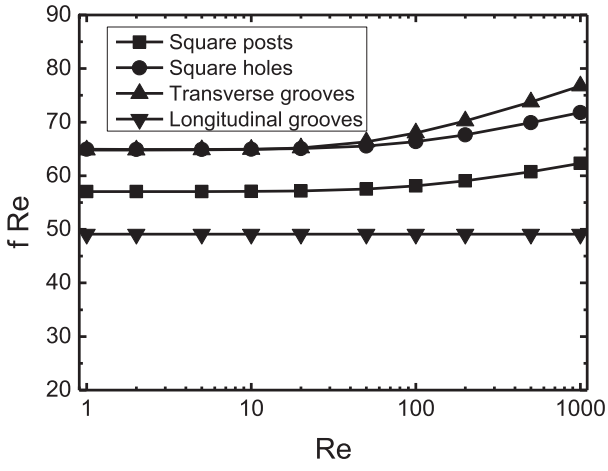

(b) $\delta_g = 0.75$

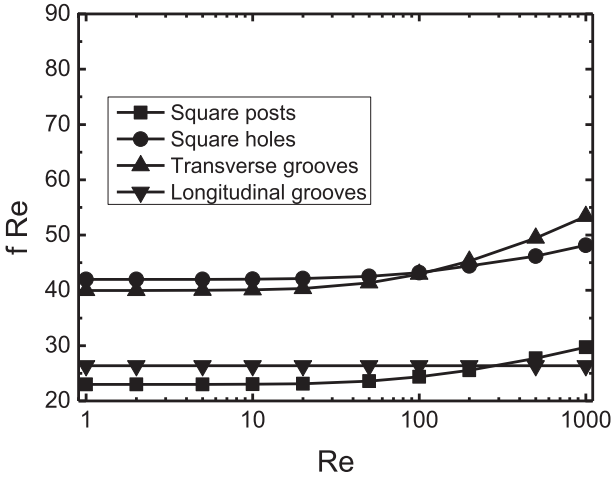

(c) $\delta_g = 0.95$

Fig. 5. Influence of Reynolds number on friction for four surface patterns at $L = 1.0$.

grooves. Fig. 5 shows the influence of Reynolds number on the friction in microchannels with the square post-, square hole-, transverse groove- and longitudinal groove-geometries corresponding to shear-free fractionδ_g = 0.5, 0.75 and 0.95 at relative pattern width $L = 1.0$. It can be observed that with the increasing Reynolds number, *fRe* products keep almost constant under $Re < 20$, because the flow inside the microchannels can be regarded as viscous Stokes flow, and the inertial effects are not significant

compared with the viscous effects. With the increasing Reynolds number when $Re > 20$, in microchannels with square posts, square posts and transverse grooves, the inertial effects become significant, the flow undergoes spatially-periodic accelerations and decelerations at the edges of the solid patches or ribs along the flow direction, the product of friction and Reynolds numbers *fRe* exhibits a dependence on the Reynolds number. With further increase in Reynolds numbers, the flow accelerations and decelerations becomes significant, leads to larger overall frictions over the channels, and *fRe* increases more rapidly at large Reynolds numbers. However, for longitudinal grooves *fRe* always keeps constant. This is attributed to the absence of the non-linear convective acceleration term in the governing equation for the fluid momentum in fully developed flow in the channel.

3.2.3. Streamwise variation of skin friction

For further investigation, the variation of skin friction, as defined in Eq. (12), along the flow direction for four surface patterns at $Re = 100$, $L = 1.0$ and $\delta_g = 0.7$ is provided in Fig. 6. The main feature for square posts, square holes and transverse grooves is that their skin friction jumps at the edge of solid patches or ribs, and the value at the edges can be much larger than the average value. At the leading edge, the boundary layer is very thin at its early development, hence the corresponding velocity gradient is very large, and so is the skin friction. However, the microchannel with longitudinal grooves exerts an invariable friction performance along the flow direction because the flow over it is identical in every cross section. It is noted that in Fig. 6 the Fanning friction factor is adopted, which is one fourth of the Darcy friction factor in Fig. 4.

3.3. Comparison of heat transfer performance

3.3.1. Effect of the shear-free fraction

In Fig. 7 the dependence of the module-averaged Nusselt numbers on the shear-free fraction is illustrated in microchannels with square posts, square holes, transverse grooves and longitudinal grooves under three different Reynolds numbers at $L = 1.0$. It can be found that *Nu* decreases with the increasing shear-free fractions. At low values of δ_g, the average Nusselt numbers for four surface patterns are only weak function of the shear-free fraction, while at high values of the shear free fraction, the Nusselt numbers drop dramatically with increasing shear-free fractions. As expected, for $Re = 100$ and 1000 when the axial heat conduction in fluid is negligible, with the decrease of shear fraction,

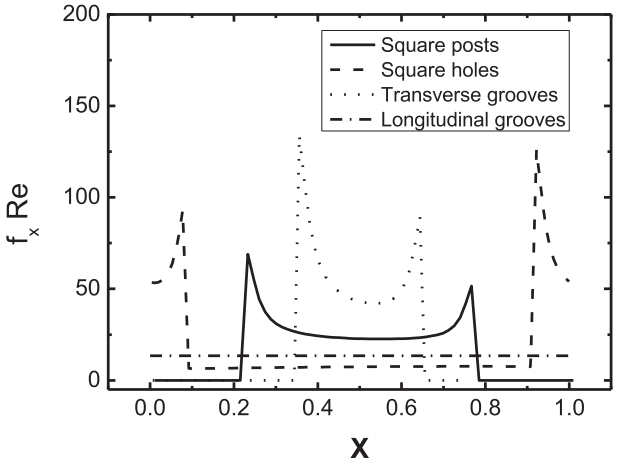

Fig. 6. Friction distribution along *X* direction at $Re = 100$, $L = 1.0$ and $\delta_g = 0.7$.

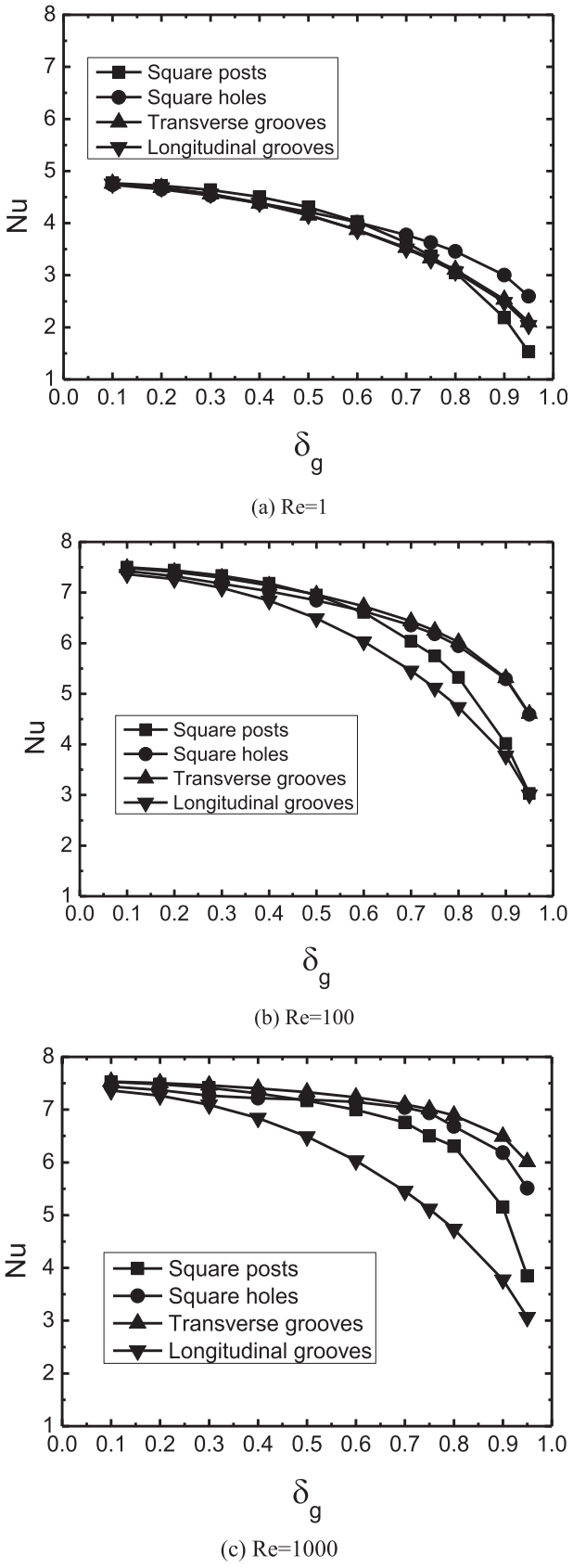

Fig. 7. Influence of shear-free fraction on Nusselt number for four surface patterns at $L = 1.0$.

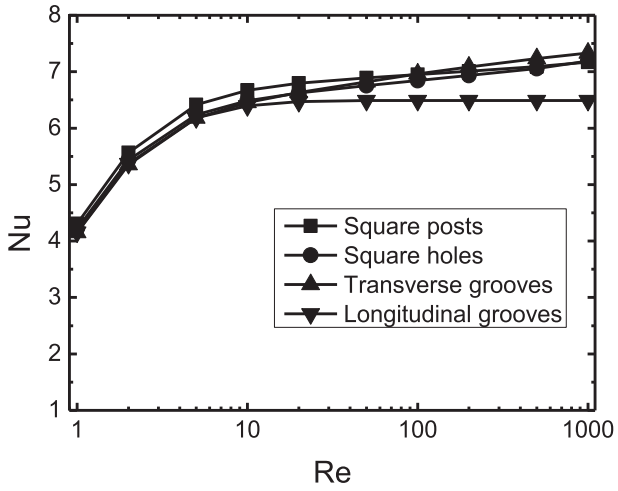

(a) $\delta_g = 0.5$

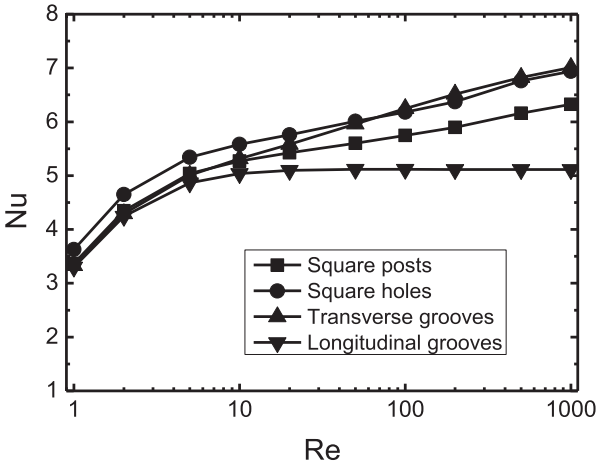

(b) $\delta_g = 0.75$

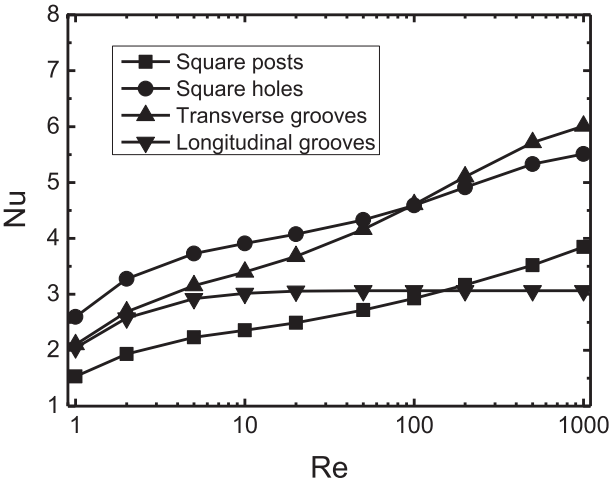

(c) $\delta_g = 0.95$

Fig. 8. Influence of Reynolds number on Nusselt number for four surface patterns at $L = 1.0$.

the Nusselt numbers approaches the value of 7.54, corresponding to fully developed laminar convective transport in a parallel plate channel at constant wall temperature.

As the Reynolds number in microchannel cooling is usually at the values of 100–200, the case at $Re = 100$ is taken as an example, as shown in Fig. 7. Due to no flow acceleration and deceleration in microchannels with longitudinal grooves, the heat transfer performance is the poorest among four surface patterns. On the contrary the heat transfer performance for the transverse grooves is the best, and the heat transfer performance for square posts and square holes are somewhere in between. As previously introduced, the two-dimensional surface patterns of square posts and square holes can be considered as the combination of one-dimensional longitudinal grooves and transverse grooves, therefore the heat transfer performance in microchannels with square posts and square holes may be close to those of longitudinal grooves and transverse grooves, especially at low or high shear-free fractions. For example at the shear-free fraction of $\delta_g < 0.5$, the non-slip region in microchannel with square posts is similar to that in the transverse grooves, so it has the equivalent Nusselt numbers as that with transverse grooves; similarly at $\delta_g > 0.9$ it has the equivalent Nusselt number as that with longitudinal groove. At the shear-free fraction of $\delta_g < 0.3$ the microchannel with the square holes has the equivalent Nusselt numbers as that with longitudinal grooves, and at $\delta_g > 0.6$ it has the equivalent Nusselt numbers as that with transverse grooves.

3.3.2. Effect of Reynolds numbers

The dependence of the module-averaged Nusselt numbers on the Reynolds numbers for four surface patterns at $\delta_g = 0.5$, 0.75 and 0.95 at $L = 1.0$ is presented in Fig. 8. For the microchannels with square posts, square holes and transverse grooves, it can be seen that with increasing Reynolds numbers, the average Nusselt numbers increase. This is because the thermal boundary layer near the solid patches or ribs becomes thinner, hence the temperature gradient there increases correspondingly, so does the total heat flux. While for the microchannel with longitudinal grooves, the Nusselt number increases with increasing Reynolds number and finally approaches a constant after $Re > 20$. This is because at reasonably high Reynolds number, the axial heat conduction in the liquid can be neglected, the average Nusselt number is only related to the convective heat transfer coefficient, which is independent of Reynolds number. However, for transverse grooves, square posts and square holes, the flow patterns are significantly affected by the

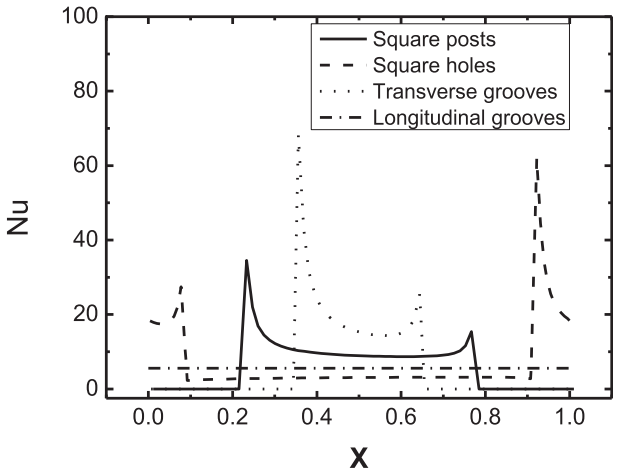

Fig. 9. Nusselt number distribution along X direction at $Re = 100$, $L = 1.0$ and $\delta_g = 0.7$.

Reynolds numbers as discussed above, so the Nusselt numbers changes strongly with the Reynolds number.

3.3.3. Streamwise variation of Nusselt numbers

In Fig. 9 the variations of local Nusselt numbers along streamwise direction in microchannels with square posts, square holes, transverse grooves and longitudinal grooves are provided at $Re = 100$, $L = 1.0$ and $\delta_g = 0.7$. The local Nusselt number is calculated with Eq. (13), which is derived from the convective heat transfer coefficient over the solid patches or grooves. Because the shear-free liquid–gas interface is considered as adiabatic, the Nusselt numbers of microchannels with square posts and transverse grooves are zero at both ends of the channels. At the leading edge of the solid patches or grooves, there is a steep increase in local Nusselt numbers, which may be attributed to the growth of the thermal boundary layer. Similar phenomenon appears near the trailing edge of the solid patches or grooves, which may be caused by the local fluid deceleration in the transition between the solid region and the following shear-free region. It is noted that the jump of Nusselt numbers are more significant at the leading edge than those in the trailing edges. When compared with Fig. 6, the local Nusselt numbers show the similar trend along streamwise direction as the skin frictions.

3.4. Comparison of goodness factor

From the above analysis on the friction and thermal performance in micro-channels with superhydrophobic surfaces, it is shown that with the increasing shear-free fraction both the friction and average Nusselt number decrease. Here a question may arise regarding how to evaluate the overall performance of the microchannels patterned with different surface geometries. Here the 'goodness factor' proposed by London [33] is introduced, which is defined as

$$\Phi = \frac{j}{f} = \frac{Nu}{fRePr^{1/3}} \tag{15}$$

and it is taken as a measure of the combined hydrodynamic and thermal effect of the superhydrophobic surfaces. For the fully developed laminar flow in a parallel-plate channel at constant wall temperature, the goodness factor is a constant

$$\Phi_c = \frac{Nu_c}{f_c Re_c Pr^{1/3}} = \frac{7.54}{96*7^{1/3}} \tag{16}$$

Here the parallel-plate channel is taken as the reference to evaluate the performance of microchannels with superhydrophobic surface patterns. When $\Phi/\Phi_c > 1$, the heat transfer enhancement over the straight smooth channel is achieved under the identical pumping power consumption.

3.4.1. Effect of shear-free fractions

Fig. 10 shows the dependence of the ratio of goodness factor Φ/Φ_c on the variation of shear-free fractions at $L = 1.0$. Although both the Nusselt numbers and frictions decrease with the increasing shear-free fractions, it is very exciting to find that the ratios of Φ/Φ_c always increase, and they are always greater than unity at $Re = 100$

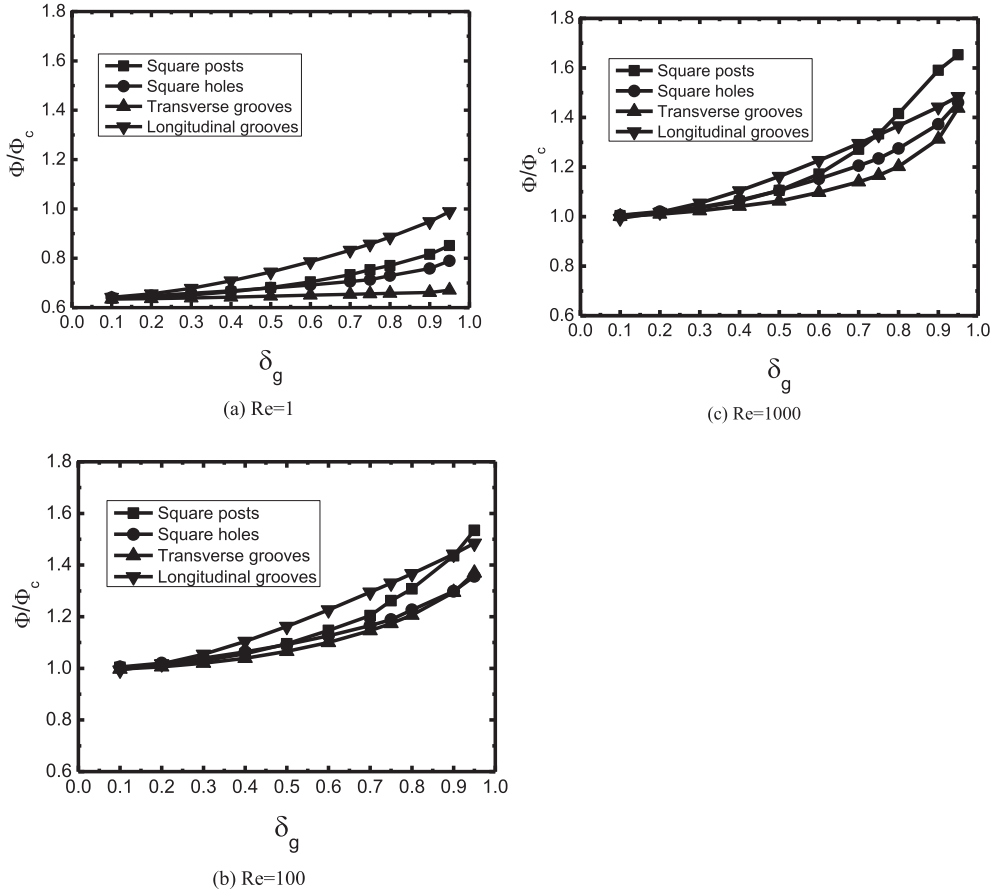

Fig. 10. Influence of shear-free fraction on Φ/Φ_c for four surface patterns at $L = 1.0$.

and 1000, which suggests overall advantage over the smooth microchannels.

For flows with Reynolds number at the order of 100, the microchannels with longitudinal grooves have higher ratio of goodness factor Φ/Φ_c than those with other three surface patterns for moderate shear-free fractions, and thus serves as a promising surface pattern for microchannel cooling. While at very high shear-free fraction $\delta_g > 0.9$, the microchannel with square posts has the highest ratio of goodness factor. It is noted that transverse groove always has the lowest Φ/Φ_c in the variation range of shear-free fractions.

3.4.2. Influence of Reynolds numbers

The variation of ratio of goodness factor Φ/Φ_c with Reynolds number at $\delta_g = 0.5$, 0.75 and 0.95 at $L = 1.0$ is provided in Fig. 11. It is found that at low Reynolds numbers the values of Φ/Φ_c is always lower than unity, which indicates the disadvantage of super-hydrophobic surface patterns over the smooth plain surface. Since the heat transfer performance under such low Reynolds number is very poor, these operating conditions are seldom applied in microchannel cooling.

With the increasing Reynolds numbers, the ratios of goodness factors Φ/Φ_c for four surfaces patterns will increase significantly first and then mildly. The ratio becomes larger than unity when Reynolds number is of order 10, which means the four surface patterns can perform better than the smooth plain surface for most general flow conditions. It is found that at $\delta_g = 0.95$ there are peaks for transverse grooves and square holes at around $Re = 500$. This is because at such high Reynolds number, the increase rate of friction is more than that of Nusselt number, leading to decreasing goodness factor.

At low to moderate shear-free fractions, i.e., $\delta_g = 0.5$ and 0.75, the microchannel with longitudinal grooves always has the highest Φ/Φ_c, while that with transverse grooves has the lowest values. At $\delta_g = 0.5$ the microchannel with square posts almost has the equivalent ratio of goodness factors as that with square holes throughout the variation range of Reynolds number, while at $\delta_g = 0.75$ the microchannel with square posts has higher ratio of goodness factors. At $\delta_g = 0.95$ the value Φ/Φ_c of microchannel with longitudinal grooves is surpassed by that of square posts at $Re > 50$.

4. Conclusion

Numerical simulations are conducted to investigate the flow and thermal transport in straight micro-channels with surfaces patterned with square posts, square holes, transverse and longitudinal grooves. The influence of shear-free fractions and Reynolds numbers on frictional and thermal performance is studied in details; the combined frictional and thermal performance is also evaluated in terms of a goodness factor. The main conclusions are summarized as follows:

1. With the increasing shear-free fraction, both the friction and module-averaged Nusselt number in microchannels for four surface patterns decrease, whereas the goodness factor which reflects the combined frictional and thermal performance increases.
2. With increasing Reynolds numbers, the average Nusselt numbers in microchannel with square posts, square holes, transverse grooves increase consistently, and the products of friction factor and Reynolds number keep constant first and then increase. The Nusselt number in microchannel with

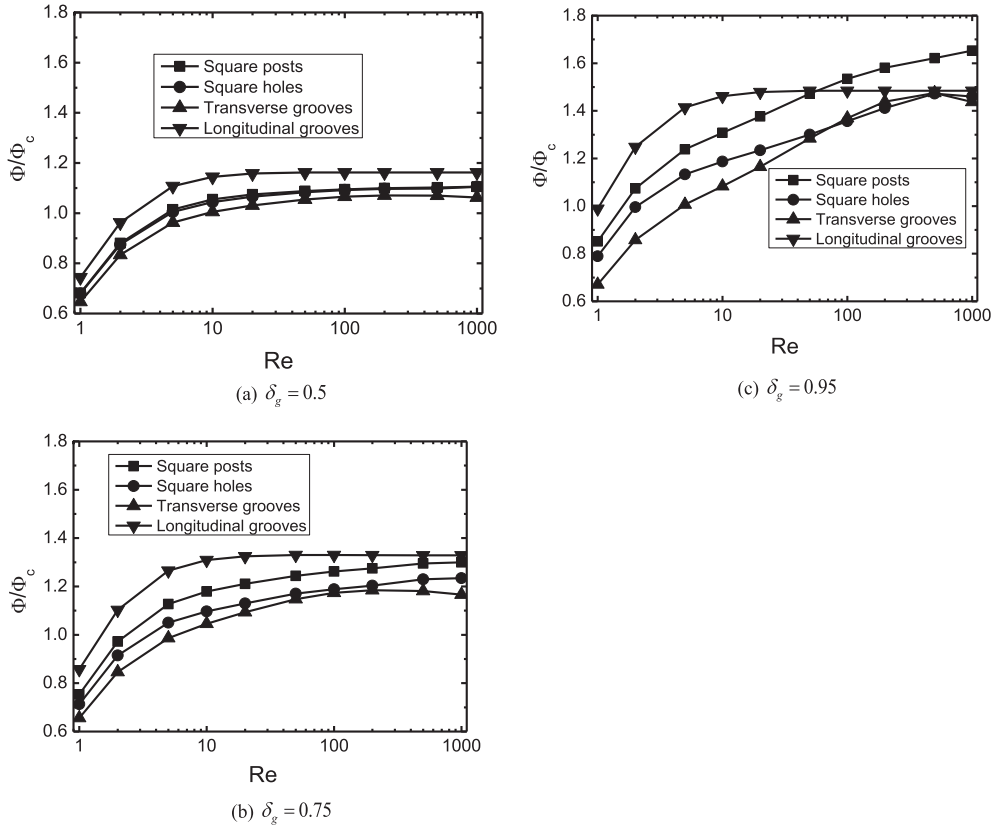

Fig. 11. Influence of Reynolds number on Φ/Φ_c for four surface patterns at $L = 1.0$.

longitudinal grooves increases first and approaches a constant, and *fRe* is always a constant. The goodness factors increases rapidly first and then mildly, even approaches constant values for all surface patterns considered.

3. The two-dimensional square posts and holes can be considered as the combination of one-dimensional longitudinal grooves and transverse grooves. At low shear-free fraction or high shear-free fraction, the square posts and square holes may exhibit the one-dimensional frictional and heat transfer performance as longitudinal and transverse grooves.
4. In general, the microchannel with transverse grooves has the lowest relative goodness factors, and that with longitudinal grooves own the highest relative goodness factor, except at high shear-free fractions and high Reynolds numbers, where they are surpassed by square posts.

The present study suggests the microchannels with superhydrophobic surfaces as promising candidates for incorporation into efficient cooling devices, where the friction is very high. Future work should include carrying out systematic experiments to validate the results of the present numerical predictions.

Acknowledgements

This research was supported by Fundamental Research Funds for the Central Universities under Grant No. JB2014239. Y.S. acknowledges the SEMS/QMUL start-up grant, and the financial support from the European Community Seventh Framework Programme under the Contract No. FP7-2010-IRSES-269205.

References

[1] A. Bar-Cohen, A.D. Kraus, S.F. Davidson, Thermal frontiers in the design and packaging of microelectronic equipment, J. Mech. Eng. 105 (1983) 53–59.
[2] D.B. Tuckerman, R.F.W. Pease, High-performance heat sinking for VLSI, IEEE Electron Device Lett. 2 (5) (1981) 126–129.
[3] S.V. Garimella, C.B. Sobhan, Transport in microchannels – a critical review, Annu. Rev. Heat Transfer 13 (2003) 1–50.
[4] I. Hassan, P. Phutthavong, M. Abdelgawad, Microchannel heat sinks: an overview of the state-of-the-art, Microscale Therm. Eng. 8 (2004) 183–205.
[5] Y. Sui, C.J. Teo, P.S. Lee, Y.T. Chew, C. Shu, Fluid flow and heat transfer in wavy microchannels, Int. J. Heat Mass Transfer 53 (2010) 2760–2772.
[6] Y. Sui, P.S. Lee, C.J. Teo, An experimental study of flow friction and heat transfer in wavy microchannels with rectangular cross section, Int. J. Therm. Sci. 50 (2011) 2473–2482.
[7] Y. Sui, C.J. Teo, P.S. Lee, Direct numerical simulation of fluid flow and heat transfer in periodic wavy channels with rectangular cross-sections, Int. J. Heat Mass Transfer 55 (2012) 73–88.
[8] Z.Y. Zheng, D.F. Fletcher, B.S. Haynes, Chaotic advection in steady laminar heat transfer simulations: periodic zigzag channels with square cross-sections, Int. J. Heat Mass Transfer 57 (2013) 274–284.
[9] D. Heymann, D. Pence, V. Narayanan, Optimization of fractal-like branching microchannel heat sinks for single-phase flows, Int. J. Therm. Sci. 49 (2010) 1383–1393.
[10] P. Xu, X.Q. Wang, A.S. Mujumdar, C. Yap, B.M. Yu, Thermal characteristics of three-shaped microchannel news with/without loops, Int. J. Therm. Sci. 48 (2009) 2139–2147.
[11] J.C. Kurnia, A.P. Sasmito, A.S. Mujumdar, Numerical investigation of laminar heat transfer performance of various cooling channel designed, Appl. Therm. Eng. 31 (2011) 1293–1304.
[12] R. Philip, Flows satisfying mixed no-slip and no-shear conditions, Z. Angew. Math. Phys. 23 (1972) 353–372.
[13] R. Philip, Integral properties of flows satisfying mixed no-slip and no-shear conditions, Z. Angew. Math. Phys. 23 (1972) 960–968.
[14] J. Ou, J.P. Rothstein, Direct velocity measurements of the flow past drag-reducing ultrahydrophobic surfaces, Phys. Fluids 17 (2005) 103606.
[15] D. Maynes, K. Jeffs, B. Woolford, W. Webb, Laminar flow in a microchannel with hydrophobic surface patterned microribs oriented parallel to the flow direction, Phys. Fluids 19 (2007) 093603.
[16] E. Lauga, H. Stone, Effective slip in pressure-driven stokes flow, J. Fluid Mech. 489 (2003) 55–77.
[17] C. Cottin-Bizonne, C. Barentin, E. Charlaix, L. Bocquet, J.L. Barrat, Dynamics of simple liquids at heterogeneous surfaces: molecular-dynamics simulations and hydrodynamic description, Eur. Phys. J. E 15 (2004) 427–438.
[18] N.V. Priezjev, A.A. Darhuber, S.M. Troian, Slip behavior in liquid films on surfaces of patterned wettability: comparison between continuum and molecular dynamics simulations, Phys. Rev. E 71 (2005) 041608.
[19] C.J. Teo, B.C. Khoo, Analysis of Stokes flow in microchannels with superhydrophobic surfaces containing a periodic array of micro-grooves, Microfluid. Nanofluid. 7 (2009) 353–382.
[20] J. Davies, D. Maynes, B.W. Webb, B. Woolford, Laminar flow in a microchannel with superhydrophobic walls exhibiting transverse ribs, Phys. Fluids 18 (2006) 087110.
[21] C.Y. Wang, Flow over a surface with parallel grooves, Phys. Fluids 15 (2003) 1114–1121.
[22] C.H. Choi, U. Ulmanella, J. Kim, C.M. Ho, C.J. Kim, Effective slip and friction reduction in nano-grated superhydrophobic microchannels, Phys. Fluids 18 (2006) 087105.
[23] C.H. Choi, C.J. Kim, Large slip of aqueous liquid flow over a nano-engineered superhydrophobic surface, Phys. Rev. Lett. 96 (2006) 066001.
[24] C. Lee, C.H. Choi, C.J. Kim, Structured surfaces for a giant liquid slip, Phys. Rev. Lett. 101 (2008) 064501.
[25] C. Ybert, C. Barentine, C. Cottin-Bizonne, P. Joseph, L. Bocquet, Achieving large slip with superhydrophobic surfaces: scaling laws for generic geometries, Phys. Fluids 19 (2007) 123601.
[26] M. Sbragaglia, K. Sugiyama, Boundary induced nonlinearity at small Reynolds numbers, Phys. D 228 (2007) 140–147.
[27] Y.P. Cheng, C.J. Teo, B.C. Khoo, Microchannel flows with superhydrophobic surfaces: effects of Reynolds number and pattern width to channel height ratio, Phys. Fluids 21 (2009) 122004.
[28] D. Maynes, B.W. Webb, J. Davies, Thermal transport in a microchannel exhibiting ultrahydrophobic microribs maintained at constant temperature, J. Heat Transfer 130 (2008) 022402.
[29] S.V. Patankar, Numerical Heat Transfer and Fluid Flow, Hemisphere, Washington, DC, 1980.
[30] W.Q. Tao, Numerical Heat Transfer, second ed., Xi'an Jiaotong University Press, Xi'an, China, 2001.
[31] Z.Y. Li, W.Q. Tao, A new stability-guaranteed second-order difference scheme, Numer. Heat Transfer B 42 (2002) 349–365.
[32] Y.P. Cheng, T.S. Lee, H.T. Low, W.Q. Tao, Improvement of SIMPLER algorithm for incompressible flow on collocated grid system, Numer. Heat Transf. B 51 (2007) 463–486.
[33] A.L. London, Compact heat exchanger, ASME Mech. Eng. 86 (1964) 31–34.